Improved Pediatric MR Imaging with Compressed Sensing[1]

Shreyas S. Vasanawala, MD, PhD
Marcus T. Alley, PhD
Brian A. Hargreaves, PhD
Richard A. Barth, MD
John M. Pauly, PhD
Michael Lustig, PhD

Purpose: To develop a method that combines parallel imaging and compressed sensing to enable faster and/or higher spatial resolution magnetic resonance (MR) imaging and show its feasibility in a pediatric clinical setting.

Materials and Methods: Institutional review board approval was obtained for this HIPAA-compliant study, and informed consent or assent was given by subjects. A pseudorandom k-space undersampling pattern was incorporated into a three-dimensional (3D) gradient-echo sequence; aliasing then has an incoherent noiselike pattern rather than the usual coherent fold-over wrapping pattern. This k-space–sampling pattern was combined with a compressed sensing nonlinear reconstruction method that exploits the assumption of sparsity of medical images to permit reconstruction from undersampled k-space data and remove the noiselike aliasing. Thirty-four patients (15 female and 19 male patients; mean age, 8.1 years; range, 0–17 years) referred for cardiovascular, abdominal, and knee MR imaging were scanned with this 3D gradient-echo sequence at high acceleration factors. Obtained k-space data were reconstructed with both a traditional parallel imaging algorithm and the nonlinear method. Both sets of images were rated for image quality, radiologist preference, and delineation of specific structures by two radiologists. Wilcoxon and symmetry tests were performed to test the hypothesis that there was no significant difference in ratings for image quality, preference, and delineation of specific structures.

Results: Compressed sensing images were preferred more often, had significantly higher image quality ratings, and greater delineation of anatomic structures ($P < .001$) than did images obtained with the traditional parallel reconstruction method.

Conclusion: A combination of parallel imaging and compressed sensing is feasible in a clinical setting and may provide higher resolution and/or faster imaging, addressing the challenge of delineating anatomic structures in pediatric MR imaging.

Supplemental material: *http://radiology.rsna.org/lookup/suppl/doi:10.1148/radiol.10091218/-/DC1*

[1] From the Departments of Pediatric Radiology (S.S.V., R.A.B.) and Radiology (B.A.H.), Stanford University School of Medicine, 725 Welch Rd, Room 1679, Stanford, CA 94305-5913; and Department of Electrical Engineering, Stanford University, Stanford, Calif (M.T.A., J.M.P., M.L.). Received July 7, 2009; revision requested September 9; final revision received December 14; accepted January 18, 2010; final version accepted February 15. **Address correspondence to** S.S.V. (e-mail: *vasanawala@stanford.edu*).

©RSNA, 2010

Magnetic resonance (MR) imaging offers superb soft-tissue characterization with global anatomic assessment, has no ionizing radiation (1), and, thus, has the potential to be a dominant pediatric imaging modality. However, a major limitation of MR imaging is slow imaging speed relative to computed tomography (CT). The resulting motion artifacts and frequent need for anesthesia often result in preference by radiologists and referring clinicians for CT, given its relative ease of use and robustness (2).

A method of increasing imaging speed in MR imaging is parallel imaging, which allows use of the varying spatial sensitivities of coils in an array to simultaneously extract spatial information that is traditionally acquired sequentially with magnetic field gradients (3–5). Over the past few years, parallel imaging has become a mainstream clinical approach that has reduced examination times and has had a substantial effect on pediatric imaging, particularly of the abdomen and cardiovascular system. Currently, two approaches to parallel imaging dominate the field: the sensitivity encoding, or SENSE, and the generalized autocalibrating partially parallel acquisition (GRAPPA) methods (6,7). Sensitivity encoding is known to have superior signal-to-noise ratio (SNR) performance, whereas GRAPPA and other autocalibration variations of it tend to be more robust in situations where it is difficult to obtain accurate coil sensitivity maps (8). However, in our practice, with our eight-channel coils at 1.5-T field strength, either approach is limited to acceleration factors of less than two on the basis of our personal experience.

This limitation has two causes. First, image SNR suffers as a consequence of the faster imaging time (6). This factor becomes an increasing concern with higher acceleration factors that approach the number of coil elements. The second is that the phased-array receive coils used for data acquisition should be designed such that each coil in the array detects signal from a relatively small volume of the imaging field of view (FOV) that differs from that detected by other coils in the array. In other words, the coil sensitivities should be optimized to the size of the patient. For pediatric imaging, this condition is often lacking, as most of the MR imaging phased-array coils are designed with adults in mind.

Another development in relation to this work is lossy image compression technology. Necessitated by teleradiology and large imaging data sets, researchers in various studies have investigated the acceptability of lossy image compression. In these studies, researchers found that high compression ratios, in excess of 8:1, can be achieved without perceptible degradation of image quality (9–12). Although these methods help diminish time for electronic transfer of images, they do not directly reduce the time required for acquisition of the images. However, because investigators in studies have validated that highly compressed images remain diagnostically useful (such as with abdominal CT scans), this finding provides evidence that medical images are compressible (ie, they have far less information in them than we attempt to collect). Moreover, the results of work suggest that rather than collecting extensive image data only to discard it in the compression process, diagnostic images can be reconstructed from markedly undersampled data, thereby increasing the speed of image acquisition (13,14). This method is referred to as *compressed sensing*. Whereas parallel imaging exploits coil sensitivity information, compressed sensing has a completely separate premise of image compressibility.

Heuristically, the overall idea is to sample k-space in a near-random fashion such that acceleration results in an aliasing pattern that is incoherent and noiselike rather than as a coherent fold-over artifact. Then this noiselike pattern, which is not compressible, can be suppressed by enforcing imaging compressibility. To implement this approach, we required a method of parallel imaging reconstruction that can (i) handle arbitrary k-space trajectories and (ii) allow introduction of various constraints to the image reconstruction. To this end, we proposed a method called iterative self-consistent parallel imaging reconstruction (SPIR-iT) (15,16). SPIR-iT exhibits better SNR performance than does conventional parallel imaging methods. It permits image reconstruction from arbitrary k-space

Advances in Knowledge

- Parallel imaging and compressed sensing can be combined.
- Combined parallel imaging and compressed sensing at high acceleration factors, compared with parallel imaging alone, showed aesthetic improvement in delineation of 162 of 325 anatomic structures, with 89 structures delineated to a greater degree.

Implication for Patient Care

- Combining parallel imaging and compressed sensing makes near-isotropic imaging at submillimeter resolution feasible.

Published online before print
10.1148/radiol.10091218

Radiology 2010; 256:607–616

Abbreviations:
FOV = field of view
GRAPPA = generalized autocalibrating partially parallel acquisition
L1 SPIR-iT = L1 norm penalized SPIR-iT
SNR = signal-to-noise ratio
SPIR-iT = iterative self-consistent parallel imaging reconstruction
3D = three-dimensional

Author contributions:
Guarantor of integrity of entire study, S.S.V.; study concepts/study design or data acquisition or data analysis/interpretation, all authors; manuscript drafting or manuscript revision for important intellectual content, all authors; approval of final version of submitted manuscript, all authors; literature research, S.S.V., R.A.B., M.L.; clinical studies, S.S.V., M.T.A., B.A.H., R.A.B., M.L.; statistical analysis, S.S.V.; and manuscript editing, S.S.V., M.T.A., B.A.H., R.A.B., M.L.

Funding:
This research was supported by the National Institutes of Health (grant NIH P41 RR09784).

See Materials and Methods for pertinent disclosures.

Radiology

sampling trajectories and provides a framework for incorporating compressed sensing (17,18).

The aim of this work was to develop a method that combines parallel imaging and compressed sensing to enable faster and/or higher-resolution MR imaging and to show its feasibility in a pediatric clinical setting. To do so, we developed a notion of image sparsity in the context of parallel imaging and incorporated it into the SPIR-iT algorithm. We call the resulting integrated method L1 norm penalized SPIR-iT (L1 SPIR-iT). Because this method is premised on a notion of image sparsity, it is not clear a priori how well anatomic structures will be delineated nor whether it offers an advantage over reconstruction premised on parallel imaging alone. Thus, our purpose was to develop a method that combines parallel imaging and compressed sensing to enable faster and/or higher spatial resolution MR imaging and to show its feasibility in a pediatric clinical setting.

Materials and Methods

GE Healthcare (Milwaukee, Wis) provides salary support for two authors (S.S.V., M.T.A.) of this article for the overall purpose of developing solutions to pediatric MR imaging problems.

Autocalibrating Parallel Imaging with SPIR-iT

SPIR-iT is an autocalibrating parallel imaging reconstruction method. It is a generalization of the GRAPPA method. In SPIR-iT, an interpolation kernel is calibrated from a fully sampled calibration area in the center of k-space. The missing k-space samples are reconstructed by iteratively applying the interpolation while enforcing data consistency with the acquired k-space data. This is mathematically represented by the following linear equations:

$$Gx = x,$$

and

$$x|_{acq} = y,$$

Table 1

Examination Specifications for Each Examination Type

Parameters	Chest MR Angiography	Abdominal MR Angiography	Extremity MR Angiography	Extremity MR Venography	Abdominal Examination	MRCP	Knee Cartilage Examination
No. of examinations	11	2	1	1	6	5	8
Mean patient age (y)	12.1 (5–17)	3.5 (3–4)	5	0	8.0 (2–17)	3.4 (2–4)	11.3 (5–17)
Mean voxel size (mm^3)	1.43 (0.77–2.75)	0.91 (0.85–0.96)	0.52	1.1	2.37 (1.17–4.79)	0.46 (0.40–0.68)	0.6581 (0.5469–0.7143)
Mean volumetric coverage (cm^3)	13 259 (7527–18 514)	9584 (9232–9935)	4300	6750	12 037 (8125–18 720)	5126 (4427–5365)	1675 (1054–2212)
Mean outer acceleration factors	4.12 (4–5.29)	4 (4,4)	4	4	4.67 (4–6)	4.62 (4–6.25)	4.24 (4–5.29)
Contrast agent dose (mmol/kg)*	0.2	0.2	0.2	0.2	0.1	NA	NA
Flip angle (degrees)	25	25	25	15	15	50	35
Echo time (msec)†	Minimum	Minimum	Minimum	Minimum	Minimum	Minimum full	5
Repetition time (msec)	Minimum	Minimum	Minimum	Minimum	Minimum	Minimum	35
Bandwidth (kHz)	65	65	65	65	65	(100–125)	32

Note.—Numbers in parentheses are ranges. MRCP = MR cholangiopancreatography, NA = not available.

* The contrast agent was gadopentetate dimeglumine (Magnevist; Bayer HealthCare, Leverkusen, Germany).

† Minimum echo time is the shortest echo time by using a fractional echo. Minimum full is the shortest echo time by using a full echo.

Table 2

Examination Rating Scales

Image Quality	Radiologist's Preference	Structure Visualization
Nondiagnostic	L1 SPIR-iT superior to parallel imaging	Seen with L1 SPIR-iT versus not seen with parallel imaging
Limited, no repeat	L1 SPIR-iT equivalent to parallel imaging	More delineation with L1 SPIR-iT than with parallel imaging
Good quality	L1 SPIR-iT inferior to parallel imaging	Aesthetic improvement with L1 SPIR-iT compared with parallel imaging
...	...	Equivalent with L1 SPIR- iT and parallel imaging
...	...	Aesthetic worsening with L1 SPIR-iT compared with parallel imaging
...	...	Less delineation with L1 SPIR-iT than with parallel imaging
...	...	Not seen with L1-SPIRIT versus seen with parallel imaging

where the operator G is the interpolation operator that is obtained from the calibration, x is the entire k-space, and y represents the acquired k-space data points.

Compressed Sensing

Several criteria must be met for successful compressed sensing. First, the underlying images should be compressible in some transform domain (eg, here we use the wavelet transform which is known to sparsely represent image data and is used in state-of-the-art image compression algorithms). Second, the artifacts in linear reconstructions (such as GRAPPA) should be incoherent (ie, there should be no anatomically recognizable ghosts). This criterion can be achieved, for example, by randomly undersampling k-space. Finally, the reconstruction should enforce sparsity. The compressed sensing reconstruction in the literature (19,20) solves the following optimization:

$$\text{minimize } ||\Psi m||_1;$$

$$\text{subject to: } F_u w = y,$$

where Ψ is a wavelet transform operator, m is the image to reconstruct, F_u is the undersampled Fourier transform, and w is the wavelet coefficient. The objective minimizes the L1 norm of the transformed image, which is known to enforce sparsity (14). The constraint enforces that the reconstructed image is consistent with the data that is acquired.

L1 SPIR-iT

Compressed sensing and SPIR-iT were synergistically combined by addressing the requirements of compressed sensing to fit within the SPIR-iT reconstruction framework.

Joint sparsity.—SPIR-iT, like GRAPPA, reconstructs the individual coil images. The sparse transforms (here, wavelet) of the individual images are correlated. To exploit that information, the L1 penalty was modified to a joint sparsity functional that takes this correlation into account. The usual definition of the L1 norm is the sum of absolute values of all the transform coefficients, $\sum_c \sum_r |w_{cr}|$, where c is the coil index and r is the position. Instead, the L1 norm was redefined to a joint L1-norm, $\sum_r \left[\sum_c |w_{cr}|^2\right]^{1/2}$.

Incoherent sampling.—Random sampling provides the high degree of incoherence needed for compressed sensing. However, it is not optimized for parallel imaging. Large gaps between samples that often occur increase noise and artifacts. However, sampling that is random but with the caveat that there is a minimum distance between samples is referred to as Poisson disk sampling. Sampling according to a Poisson disk distribution provides a high degree of artifact incoherence and, at the same time, uniform distance between samples (21). Poisson disk sampling also characterizes the spacing between photoreceptor cells in the eye and is responsible for the fact that the eye produces very few aliasing artifacts (22). It also provides flexibility for fractional and anisotropic acceleration, resulting in better fit to the different coil array geometries. This is particularly relevant to pediatric imaging, where there is a wide range of patient sizes and, hence, FOVs.

Nonlinear sparsity enforcing reconstruction.—The SPIR-iT and the compressed sensing reconstructions were combined as follows:

$$\text{minimize JointL1 } (\Psi m);$$

$$\text{subject to: } F_u m = y;$$

$$x = Fm$$

$$Gx = x,$$

where m is the target image, F is a fully sampled Fourier transform, and x is the reconstructed k-space.

The reconstruction is described explicitly in Appendix E1 (online).

Implementation

A standard three-dimensional (3D) spoiled gradient-recalled acquisition in the steady state sequence (18) was modified to include a Poisson disk undersampling distribution. The advantage of the Poisson disk sampling is that data can be reconstructed by using product parallel imaging reconstruction, such as autocalibrating reconstruction for cartesian sampling (ARC; GE Healthcare) (23), a variant of GRAPPA. The resulting images will be more immune to calibration error, as any residual aliasing will be incoherent (Figure E1 [online]). This aliasing can be further removed with a compressed sensing reconstruction. The L1 SPIR-iT algorithm was implemented in a software programming language (Matlab; MathWorks, Natick, Mass) by using a

Figure 1

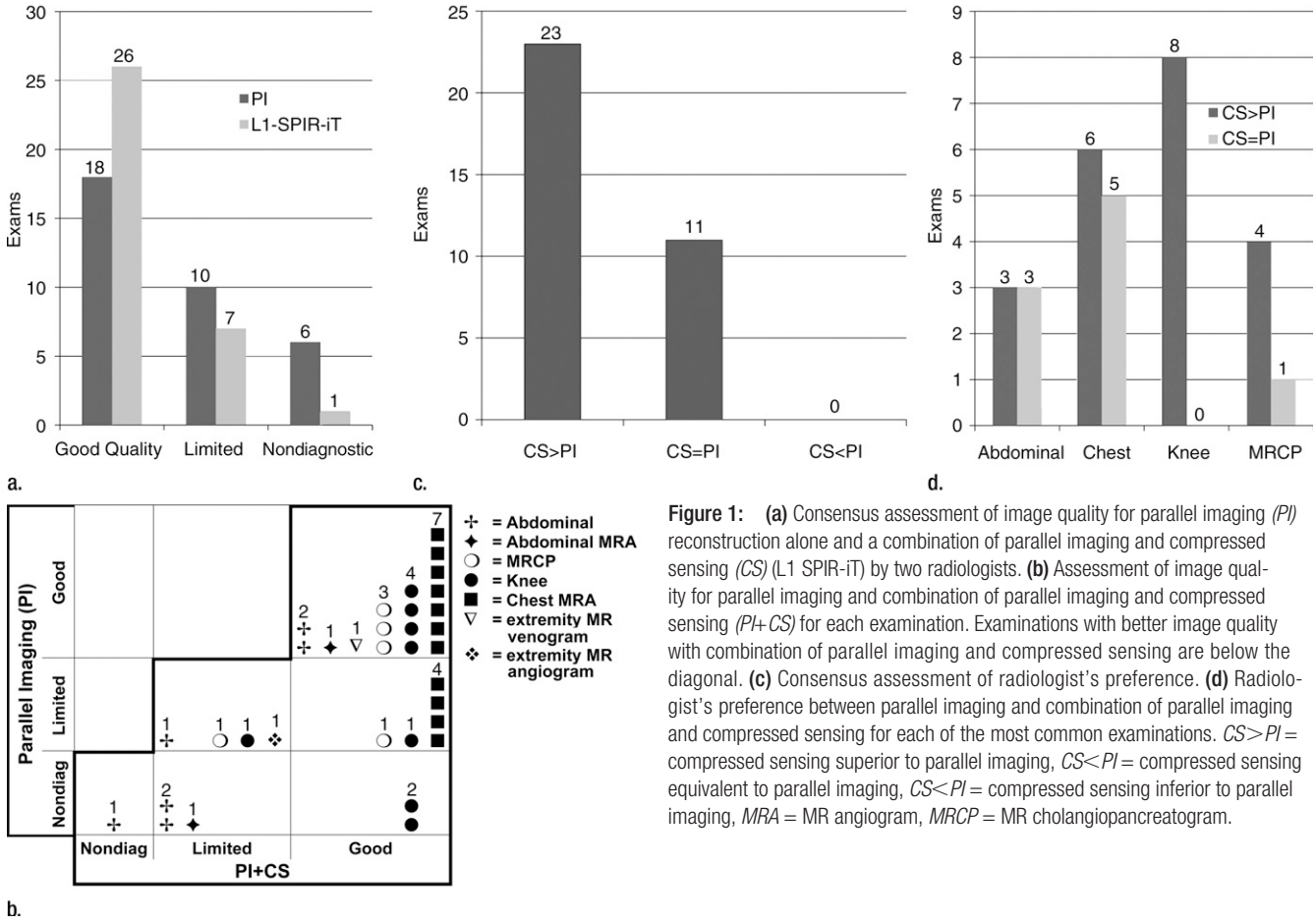

Figure 1: **(a)** Consensus assessment of image quality for parallel imaging *(PI)* reconstruction alone and a combination of parallel imaging and compressed sensing *(CS)* (L1 SPIR-iT) by two radiologists. **(b)** Assessment of image quality for parallel imaging and combination of parallel imaging and compressed sensing *(PI+CS)* for each examination. Examinations with better image quality with combination of parallel imaging and compressed sensing are below the diagonal. **(c)** Consensus assessment of radiologist's preference. **(d)** Radiologist's preference between parallel imaging and combination of parallel imaging and compressed sensing for each of the most common examinations. *CS>PI* = compressed sensing superior to parallel imaging, *CS<PI* = compressed sensing equivalent to parallel imaging, *CS<PI* = compressed sensing inferior to parallel imaging, *MRA* = MR angiogram, *MRCP* = MR cholangiopancreatogram.

projection-onto-convex-sets approach with a wavelet-sparsifying transform. This method is described in more detail elsewhere (15–17).

With institutional review board approval and informed consent or assent for this HIPAA-compliant study, we recruited patients referred for routine contrast material–enhanced cardiovascular MR imaging, contrast-enhanced abdominal MR imaging, MR cholangiopancreatography, and knee MR imaging. Recruitment for contrast-enhanced cardiovascular and abdominal examinations began in August 2008, whereas MR cholangiopancreatography and knee examination recruitment began in November and December, respectively. All recruitment ended in January 2009. The inclusion criterion was that a patient had been referred at the children's hospital for the above-mentioned types of MR examinations. The exclusion criterion for contrast-enhanced examinations was any clinical issue that was unresolved by using nonenhanced imaging that required first-pass imaging with a gadolinium-based contrast agent (10 patients). This was a convenience sample, with recruitment undertaken when investigators were available to obtain informed consent.

In each case, a single 3D spoiled gradient-recalled acquisition in the steady state with Poisson disk sampling was obtained with outer acceleration (degree of undersampling outside of the central calibration region of k-space) at least equal to the number of sensitive coils in the phase-encoding directions (two coils by two directions to 2.5 coils by 2.5 directions). Cardiovascular and abdominal acquisitions were obtained after double- and single-dose gadolinium-based contrast agent intravenous injections, respectively. The higher acceleration than what is normally used clinically was used to increase spatial resolution to obtain voxel sizes approximately half that obtained in our routine clinical examinations. Knee examinations were performed without gadolinium-based contrast agent, and the acceleration was used to decrease image time. For MR cholangiopancreatographic examinations, radiofrequency spoiling and gradient dephasing was eliminated to yield balanced state free precession images with T2 weighting. Mean voxel size, volumetric coverage, and outer

Figure 2

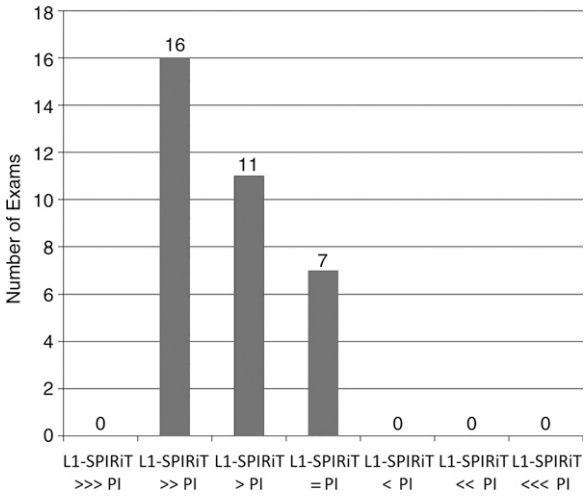

Figure 2: Overall anatomic structure visualization at examination according to image reconstruction method: L1 SPIR-iT or parallel imaging *(PI)* alone. *L1-SPIRit >>> PI* = seen with L1 SPIR-iT versus not seen with parallel imaging, *L1-SPIRit >> PI* = more delineation with L1 SPIR-iT than with parallel imaging, L1-SPIRiT > PI = aesthetic improvement with L1 SPIR-iT compared with parallel imaging, *L1-SPIRiT = PI* = equivalent with both L1 SPIR-iT and parallel imaging, *L1-SPIRiT < PI* = aesthetic worsening with L1 SPIR-iT compared with parallel imaging, *L1-SPIRiT << PI* = less delineation with L1 SPIR-iT than with parallel imaging, *L1-SPIRiT <<< PI* = not seen with L1 SPIR-iT versus seen with parallel imaging.

Table 3

Individual Structure Delineation for Most Common Examination Types

Examination Type	L1 SPIR-iT and Parallel Imaging Equivalent	Aesthetic Improvement with L1 SPIR-iT versus Parallel Imaging	More Delineation with L1 SPIR-iT versus Parallel Imaging
Chest MR angiography	29	82	17
Abdominal examination	17	36	24
MRCP	0	16	5
Knee cartilage examination	1	16	32

Note.—MRCP = MR cholangiopancreatography.

acceleration factors for each study type are shown in Table 1.

Two sets of images were then reconstructed for each subject from this single data set by using both a standard parallel imaging method (autocalibrating reconstruction for cartesian sampling [GE Healthcare]) with a 7 × 7 × 5 kernel and the above-mentioned compressed sensing (L1 SPIR-iT) method. A 7 × 7 × 5 kernel was used, along with an L1 penalty parameter of 0.015. These parameters were previously optimized on volunteer data sets. Images reconstructed by using parallel imaging alone were generated on the imager and then transferred to the picture archiving and communication system. L1 SPIR-iT images that were reconstructed in software programming language (Matlab; MathWorks) were then transferred to our picture archiving and communication system.

Two board-certified radiologists with certificates of added qualification in pediatric radiology (S.S.V. and R.A.B., with 5 and 20 years of clinical experience with MR imaging, respectively) viewed the two image series for each of 34 examinations in 34 patients (19 male and 15 female patients; mean age, 8.1 years; range, 0–17 years) side by side on our standard clinical picture archiving and communication system and assigned scores to the images in consensus. The image quality of each image series was rated (Table 2), and each image series was compared for radiologist's preference. In addition, for each examination type, a scale (Table 2) was used to compare the relative quality of delineation of specific anatomic structures (Appendix E2 [online]) that are typically evaluated for that examination type in routine clinical practice.

Statistical Analysis

Comparisons of image quality, radiologist's preference, and structure visualization between imaging methods were performed with stratified paired Wilcoxon tests, with examination type (abdomen, chest, knee, and MR cholangiopancreatography) as the strata. Differences in image quality were also tested by using an exact Bowker test of symmetry. Statistical analyses were performed with statistical software (R, version 2.9.2; *http://www.r-project.org/*) by using the "coin" package (*http://cran.r-project.org/*) for the Wilcoxon tests and software (Stata, release 9.2; StataCorp, College Station, Tex) for the symmetry tests. A difference with a *P* value of .05 was used as a criterion of significance.

Results

A total of 34 examinations were successfully completed, including 11 chest MR angiographic, two abdominal MR angiographic, one extremity MR angiographic, one extremity MR venographic, six abdominal, five MR cholangiopancreatographic, and eight knee cartilage examinations. The mean age for female patients was 9.3 years (range, 2–17 years), and the mean age for male patients was 7.2 years (range, 0–17 years).

A total of 10 examinations were not satisfactorily completed and, thus, were excluded from further analysis. In seven cases, the gradient-warp correction algorithm chosen for the standard parallel imaging algorithm images was noted to be different from that for the L1 SPIRiT

Figure 3

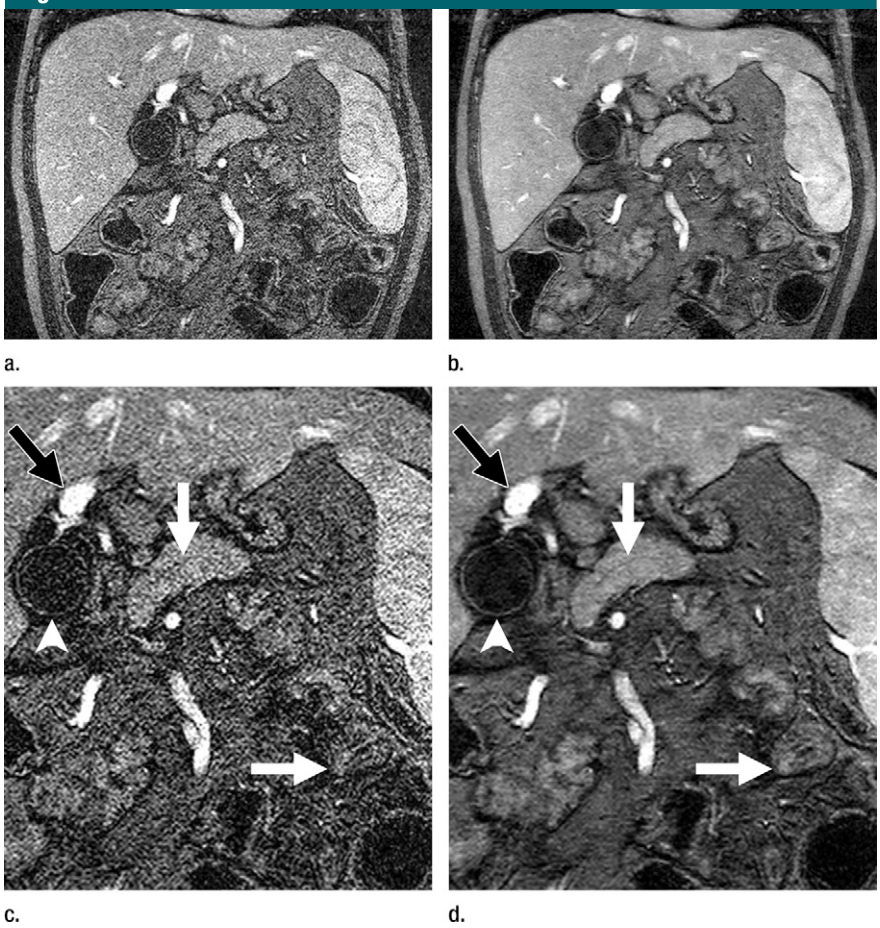

Figure 3: **(a–d)** Submillimeter near-isotropic–resolution contrast-enhanced T1-weighted MR images (repetition time msec/echo time msec, 4.7/1.4; section thickness, 2.2 mm; matrix, 384 × 384 over 30-cm FOV), with an acceleration factor of four, in 8-year-old boy. **(a, c)** Standard and **(b, d)** compressed sensing reconstruction images. **(c, d)** Zoomed images show improved delineation of the pancreatic duct (vertical arrow), bowel (horizontal arrow), and gallbladder wall (arrowhead), and equivalent definition of portal vein (black arrow) with L1 SPIR-iT reconstruction.

images; thus, anatomic structures could not be perfectly aligned for side-by-side comparison. In one case, the MR imaging examination was terminated after localizer images were obtained, owing to extensive metal artifact. In another case, the images from the examination had extensive spike noise artifact. Finally, in one case, the examination was terminated early because the patient became unstable. L1 SPIR-iT reconstruction times for the cases were approximately 80 minutes.

The results on relative image quality and radiologist's preference are summarized in Figure 1. Compressed sensing resulted in more examinations with image quality rated as good and fewer examinations with image quality rated as nondiagnostic (Wilcoxon and symmetry tests, $P < .001$). Also, compressed sensing image quality was consistently rated the same as or better than autocalibrating reconstruction for cartesian sampling image quality (Wilcoxon and symmetry tests, $P < .001$). Similarly, overall compressed sensing was preferred in 70% of examinations (Wilcoxon test, $P < .001$), with the effect appearing strongest in knee and MR cholangiopancreatographic examinations.

The results on structure delineation are summarized in Figure 2. In approximately one-half of all patients, there was greater delineation of anatomic structures with the compressed sensing approach, whereas no compressed sensing examinations included structures that were suppressed (Wilcoxon test, $P < .001$). A total of 325 structures were evaluated. Approximately one-half of all structures ($n = 162$) were believed to have aesthetic improvement, but without any greater degree of delineation (ie, image quality was improved in terms of radiologist's preference for visualization of that specific structure without distraction from noise, but no particular feature or portion of the structure was depicted to a greater extent by using one reconstruction method over the other). Overall, 89 structures were delineated to a greater degree, whereas 74 structures were equivalently delineated. Table 3 details the relative delineation of structures for the more common examination types.

Representative examples are shown in Figures 3–6. Figure 5 shows that small structures, such as peripheral pulmonary arteries, are well delineated with compressed sensing reconstruction and that soft-tissue contrast is preserved. Even higher accelerations that exceed the number of coils in the phase-encoding directions may be obtained (Figs 6, E2 [online]).

Discussion

We used a combination of parallel imaging and compressed sensing to generate images at acceleration factors that are more than double those used in our standard clinical practice. In particular, we generated and evaluated images in clinical patients from data acquired after gadolinium-based contrast agent administration. These dynamic gadolinium-enhanced images often have the highest clinical value and are the most challenging to obtain reliably in children. In so doing, we were able to achieve near-isotropic submillimeter resolution and have demonstrated that, at these levels of acceleration, compressed sensing reconstruction did not suppress anatomic detail.

Figure 4

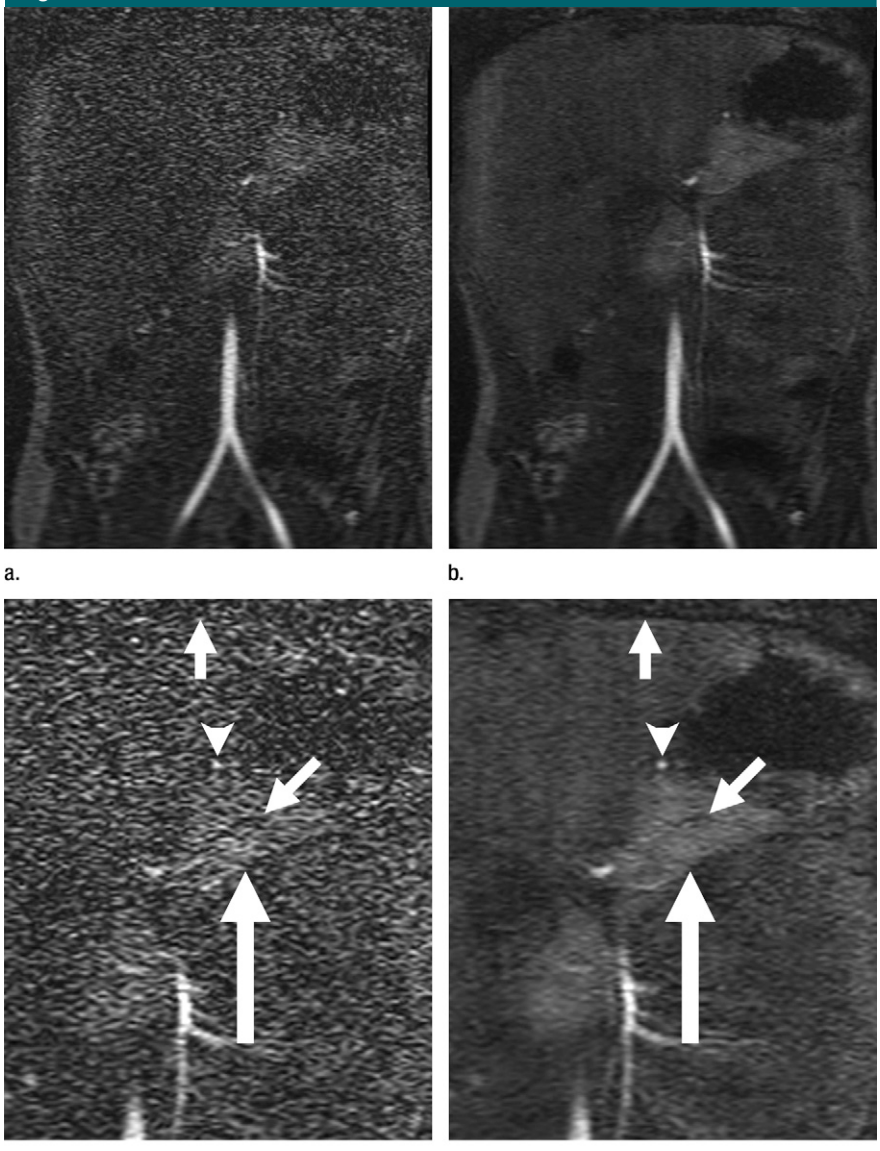

Figure 4: **(a–d)** Breath-hold gadolinium-enhanced MR angiograms (4.8/1.1; section thickness, 1.6 mm; matrix, 512 × 320 over 35-cm FOV) in 9-year-old boy with hypertension, with four times acceleration at 1.2-mm^3 resolution. **(a, c)** Images with parallel imaging alone. **(b, d)** Images with L1 SPIR-iT compressed sensing. **(c, d)** Zoomed images show improved delineation of pancreas (large arrow), pancreatic duct (middle arrow), and diaphragm (small arrow) and left gastric artery (arrowhead) emerging from the noise with L1 SPIR-iT.

Given that the compressed sensing reconstruction involves iterative nonlinear operations that favor images that are sparsely represented in the wavelet domain, it is not obvious that anatomic detail would be preserved. Validation of reconstruction methods that are based on assumptions about the underlying structure of images, such as sparsity, is challenging to achieve in phantom experiments because the phantoms fail to capture the characteristics of in vivo images. In our study, however, we demonstrated that, compared with parallel imaging alone, delineation of anatomic structures that are routinely evaluated at MR examinations that are part of our clinical practice is preserved or increased with a combination of compressed sensing and parallel imaging. Although our study is not a definitive assessment of preserved sensitivity of detection of subtle pathologic findings, the results of our study are encouraging and lend evidence that this approach to accelerating imaging may be acceptable for clinical examinations with the types of image contrast we need.

There were several limitations to our study. Although standard parallel imaging reconstruction algorithms were compared with a compressed sensing reconstruction algorithm, this comparison was performed only at high acceleration factors to test whether anatomic structures are adequately delineated. We did not compare these images to images obtained with high-acceleration compressed sensing and lower-acceleration parallel imaging. The challenge of that type of study would be twofold: Different physiologic motion between the different data acquisitions would confound the ability to compare structures. Similarly, comparison of contrast-enhanced examinations would be confounded by different time of acquisition of images relative to the intravenous contrast bolus.

Another limitation of our study was the lack of blinding of the radiologists to the type of image reconstruction. Blinding would have been difficult to achieve, as the compressed sensing images can be clearly differentiated from the standard images because they have much less noise. Quantitative measures of image quality and, in particular, SNR are often used in comparisons of image techniques. In this study, we avoided the use of these measures, as calculation of SNR in MR imaging with parallel imaging is usually not feasible in clinical situations, especially when a gadolinium-based contrast agent is administered.

A further limitation of our study was the use of only a 3D gradient-echo sequence. We used this sequence for two reasons: First, higher-dimensionality

Figure 5

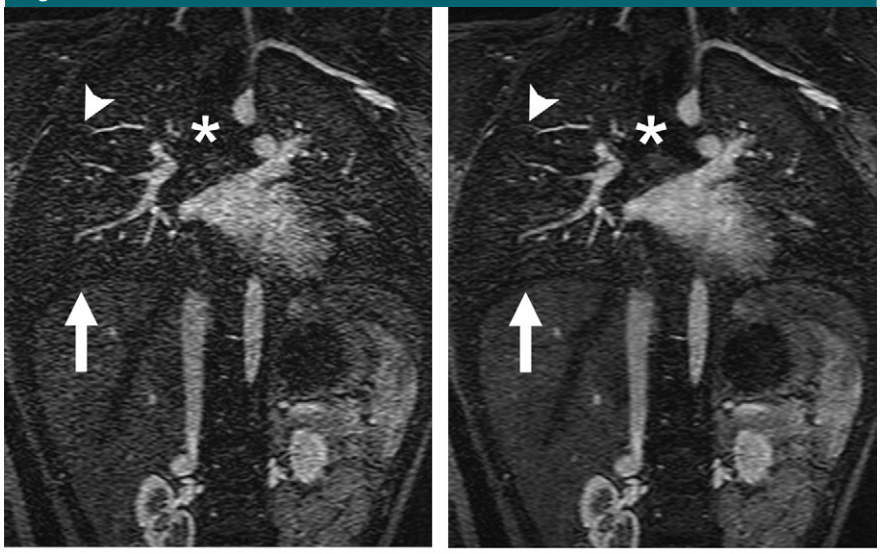

a. b.

Figure 5: **(a, b)** Thoracic MR angiograms (4.2/1.1; section thickness, 1.8 mm; matrix, 384 × 384 over 30-cm FOV) in 6-year-old girl. Coronal reformatted **(a)** parallel and **(b)** L1 SPIR-iT images of a sagittal 3D acquisition with four times outer acceleration. Note preserved subtle contrast of trachea (*) and diaphragm (arrow), as well as structural fine detail of pulmonary vessels (arrowhead).

Figure 6

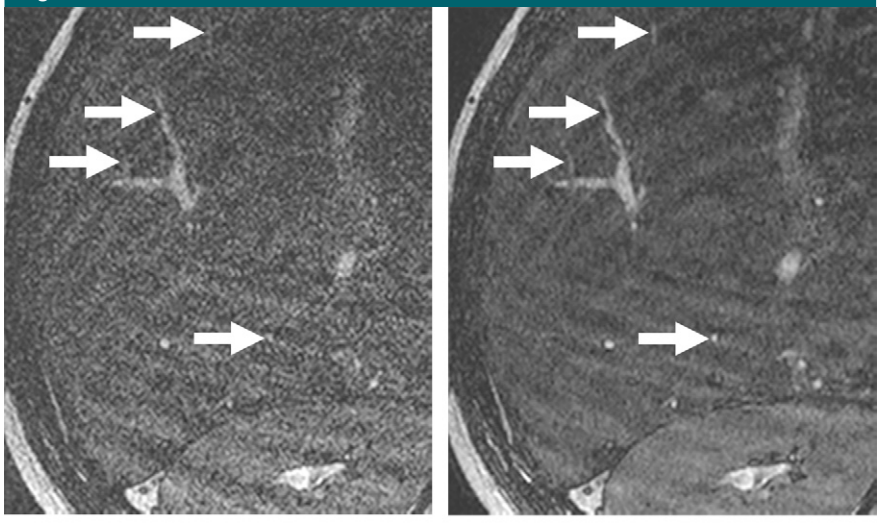

a. b.

Figure 6: **(a)** Parallel image and **(b)** compressed sensing MR cholangiopancreatogram in 3-year-old boy with left hepatic lobe transplant acquired with a 3D balanced steady state sequence (6.8/3.4; section thickness, 1.8 mm; matrix, 384 × 384 over 18-cm FOV) and eight-channel phased-array coil at 6.3-fold acceleration and 0.4-mm^3 resolution. Because only two coils are in each of the two phase-encoding directions, a traditional parallel imaging approach would have limited acceleration to at most four (two coils by two directions). Note detailed delineation of minute bile ducts, with aesthetic improvement in some ducts and greater delineation of other ducts (arrows) with **(b)** compressed sensing reconstruction versus **(a)** conventional reconstruction. With improved noise reduction, residual ghosting becomes more obvious.

data sets tend to be more compressible, so two-dimensional imaging with traditional spin-echo T2-weighted and proton-density weighted image contrast may not benefit as greatly from a compressed sensing approach. Second, modification of a 3D gradient-echo sequence to permit Poisson disk sampling is easier than it is with 3D spin-echo sequences.

Our work is preliminary and shows the feasibility of this approach at acceleration factors that are approximately double that which can be conventionally achieved. Future work should be aimed at evaluation of these techniques in larger patient cohorts for specific MR imaging examinations, such as thoracic MR angiography, and the assessment of diagnostic performance for specific diseases. Although we achieved the specific improvement of near-isotropic imaging with this technique, further gains may be achieved by refining the reconstruction method and optimizing the L1 penalty. Although wavelet encoding is the most extensively used representation for image compression and was used in the compressed sensing reconstruction for our study, other transformations that may be better suited to represent specific types of MR images should be explored. In addition, reconstruction times for this study were too long to be clinically acceptable, and future research will involve more rapid reconstruction times.

Acknowledgments: The authors thank Jarrett Rosenberg, PhD, for generous assistance with statistical analysis and Jennifer Vancil for skillful help with manuscript preparation.

References

1. Neto JA, Elazzazzi M, Altun E, Semelka RC. When should abdominal magnetic resonance imaging be used? Clin Gastroenterol Hepatol 2008;6(6):610–615.
2. Olsen OE. Imaging of abdominal tumours: CT or MRI? Pediatr Radiol 2008;38(Suppl 3):452–458.
3. Hutchinson M, Raff U. Fast MRI data acquisition using multiple detectors. Magn Reson Med 1988;6(1):87–91.
4. Kwiat D, Einav S, Navon G. A decoupled coil detector array for fast image acquisition in magnetic resonance imaging. Med Phys 1991;18(2):251–265.

5. Ra JB, Rim CY. Fast imaging using subencoding data sets from multiple detectors. Magn Reson Med 1993;30(1):142–145.

6. Pruessmann KP, Weiger M, Scheidegger MB, Boesiger P. SENSE: sensitivity encoding for fast MRI. Magn Reson Med 1999; 42(5):952–962.

7. Griswold MA, Jakob PM, Heidemann RM, et al. Generalized autocalibrating partially parallel acquisitions (GRAPPA). Magn Reson Med 2002;47(6):1202–1210.

8. Blaimer M, Breuer F, Mueller M, Heidemann RM, Griswold MA, Jakob PM. SMASH, SENSE, PILS, GRAPPA: how to choose the optimal method. Top Magn Reson Imaging 2004;15(4):223–236.

9. Goldberg MA, Gazelle GS, Boland GW, et al. Focal hepatic lesions: effect of three-dimensional wavelet compression on detection at CT. Radiology 1997;202(1):159–165.

10. Kim B, Lee KH, Kim KJ, et al. Prediction of perceptible artifacts in JPEG2000 compressed abdomen CT images using a perceptual image quality metric. Acad Radiol 2008;15(3):314–325.

11. Koff DA, Shulman H. An overview of digital compression of medical images: can we use lossy image compression in radiology? Can Assoc Radiol J 2006;57(4):211–217.

12. Ringl H, Schernthaner RE, Kulinna-Cosentini C, et al. Lossy three-dimensional JPEG2000 compression of abdominal CT images: assessment of the visually lossless threshold and effect of compression ratio on image quality. Radiology 2007;245(2): 467–474.

13. Gamper U, Boesiger P, Kozerke S. Compressed sensing in dynamic MRI. Magn Reson Med 2008;59(2):365–373.

14. Lustig M, Donoho D, Pauly JM. Sparse MRI: The application of compressed sensing for rapid MR imaging. Magn Reson Med 2007;58(6):1182–1195.

15. Lustig M. Sparse MRI. Stanford, Calif: Stanford University, 2008.

16. Lustig M, Pauly JM. Iterative grappa: a general solution for the grappa reconstruction from arbitrary k-space sampling [abstr]. In: Proceedings of the Fifteenth Meeting of the International Society for Magnetic Resonance in Medicine. Berkeley, Calif: International Society for Magnetic Resonance in Medicine, 2007; 333.

17. Lustig M, Alley MT, Vasanawala SS, Donoho DL, Pauly JM. L1 SPIR-iT: autocalibrating parallel imaging compressed sensing [abstr]. In: Proceedings of the Seventeenth Meeting of the International Society for Magnetic Resonance in Medicine. Berkeley, Calif: International Society for Magnetic Resonance in Medicine, 2009; 379.

18. Lustig M, Pauly JM. SPIR-iT: iterative self-consistent parallel imaging reconstruction from arbitrary k-space. Magn Reson Med (in press).

19. Candes E, Romberg J, Tao T. Robust uncertainty principles: exact signal reconstruction from highly incomplete frequency information. IEEE Trans Inf Theory 2006;52(2): 489–509.

20. Donoho D. Compressed sensing. IEEE Trans Inf Theory 2006;52(4)1289:1306.

21. Glassner A. An introduction to ray tracing. San Francisco, Calif: Morgan Kaufman, 1989.

22. Yellott JI Jr. Spectral consequences of photoreceptor sampling in the rhesus retina. Science 1983;221(4608):382–385.

23. Beatty P, Brau A, Chang S, et al. A method for autocalibrating 2-D accelerated volumetric parallel imaging with clinically practical reconstruction times [abstr]. In: Proceedings of the Fifteenth Meeting of the International Society for Magnetic Resonance in Medicine. Berkeley, Calif: International Society for Magnetic Resonance in Medicine, 2007; 1749.